Use of an environmental proxy to determine turbulence regime surrounding a full-scale tidal turbine deployed within the Fromveur Strait, Brittany, France.

Fowell, R.[1], Togneri, M.[2], Pacheco, A.[3], Nourrisson, O.[4]

[1]University of Plymouth, England, bfowell95@gmail.com

[2]Swansea University, Wales, m.togneri@swansea.ac.uk

[3]CIMA/Universidade do Algarve, Portugal, ampacheco@ualg.pt

[4]SABELLA S.A.S., France, o.nourrisson@sabella.bzh

Abstract

Establishing a relationship between tidal current conditions and tidal turbine performance and loads is a critically important consideration for turbine reliability. Nonetheless, obtaining in-situ information is often challenging, and as a result both environmental and load data may be more sparse than desired. This study presents a method to make use of limited data sets by establishing a relationship between measurements of hydrodynamic variability and turbine power or blade strain variability, even when these measurements are not taken simultaneously. The method is tested on data from the deployment of a full-scale pilot tidal turbine: in situ velocity measurements and turbulence characteristics taken at times when the turbine was not installed were associated with power and strain measurements during the turbine's deployment via a Delft3D proxy. The data show that the variability of active power correlates well with turbulence kinetic energy (TKE) when comparing similar populations via the proxy. Examination of blade strain variance against TKE shows a weaker correlation, with fat-tailed distributions and extremely high strain outlier values present across all flow speeds. Acceleration or deceleration of the flow influenced the power variability of the turbine, with larger standard deviations recorded across accelerating flows. No significant difference was found when comparing blade strain variance in accelerating and decelerating flows. We conclude that the proxy method studied can establish a population-level relationship between non-simultaneous environmental and load data, but that the accuracy and precision of this relationship depends on the amount of data available: this method is therefore only suitable where there is a sufficiently rich dataset.

Keywords: Tidal energy; Tidal energy convertors; Turbulence kinetic energy; Hydrodynamic modelling; Fromveur Strait; Blade strain.

1. Introduction

Increasingly across the past decade, tidal stream energy has attracted significant interest as it has established itself as a highly predictable resource, which benefits from low environmental and reduced visual impacts. Several full-scale tidal energy converters (TECs) have proven the capability of tidal stream power, including for example (i) SeaGen in Strangford Lough (Northern Ireland, UK) with the implementation of a 1.2 MW device [1], (ii) the MeyGen scheme in Pentland Firth (Northern Scotland, UK) with the implementation of four 1.5 MW horizontal-axis turbines [2] and (iii) the 2 MW floating O2 turbine implemented by Orbital Marine at the European Marine Energy Centre (EMEC) site (Orkney archipelago, UK) [3]. However, when compared to other forms of renewable energy technologies (in particular, wind and solar devices), profiting from tidal stream energy remains a challenge due to the relative immaturity of the technology and the greater expense of operations and maintenance in the significantly harsher environmental conditions that TECs operate in.

Tidal currents are typically highly turbulent, driving significant blade root flapwise and chordwise bending moments because of the velocity shear, demonstrating that a TEC's rotor experiences exceptionally high dynamic forces once deployed; when coupled with prolonged exposure, these moments largely affect the loading and subsequent reliability of the turbine [4-6]. Limited knowledge of the long-term effects of these varying hydrodynamic loads have caused tidal manufacturers to over-estimate safety coefficients, consequently increasing the levelised cost of energy (LCOE) and discouraging investment [7-8]. Parallel to this, uncertainty in the structural integrity of TECs to such dynamic loading influences the planning and timescales of operation and maintenance procedures, further increasing the LCOE. Hence, knowledge and consideration of turbulence and its impact on the loading, fatigue and subsequent efficiency of tidal turbines is essential for progressing the design and implementation of these devices and derisking the technology for investors.

Results from laboratory-scale testing have aided in the development of tidal turbine technology by providing valuable insights into fluid-instrument interactions [9-11].

However, flow conditions and turbulence characteristics found at tidal energy sites are notably different from those generated in laboratory settings and can vary significantly between deployment locations. As such, in-situ deployments of full-scale TEC prototypes are the best opportunity for a comprehensive assessment of device performance as expected in tidal energy sites. Several studies within the literature have already reported full-scale investigations into the substantial effect that turbulence has on the performance and reliability of TECs [12-15]. However, obtaining reliable, simultaneous measurements of both environmental conditions and device loading is often challenging: deployment and engineering constraints can restrict availability of hydrodynamic and device load instrumentations, instrument failures can go undetected until they are retrieved post-deployment, and data access is frequently restricted due to commercial sensitivity. These factors have not only introduced a degree of uncertainty in the testing of full-scale devices but are a key factor limiting the number of scientific reports detailing results of full-scale trials.

In this paper, we present the results of a study on the deployment of a full-scale pilot TEC (the bottom mounted D10, developed by Sabella S.A.S.) at a key tidal stream resource site in French waters. During the deployment, instrumentation on the device gathered data on power production and blade root strain. While the D10 was on site, the Nortek Signature500 five-beam acoustic Doppler current profiler (hereon in referred to as AD2CP) was also deployed to obtain a more detailed picture of the resource; in particular, the measurements from this instrument were used to characterise turbulence in the tidal current. Technical issues with the instrumentation meant that there were no times when all three data sources (power measurement, blade strain measurement and AD2CP) were operating simultaneously. Therefore, to establish a link between the variability of the resource and the variability of the device loads, a proxy Delft3D model was used to assign measurements from each instrument into several bins depending on the expected tidal current at the time of measurement. These bins contain measurements taken at times when tidal conditions were similar. Thus, although it is not possible to link any particular instant in time from the AD2CP turbulence measurements to the resultant load fluctuations on the turbine, a population-level comparison can be performed.

This study is divided into six primary sections, following this introduction. First, the test-site location, D10 controls and AD2CP deployment conditions are described in Section 2, followed by the quantification of turbulence parameters and correspondence with the

load data in Section 3. The results attained are then described and analysed in Section 4, followed by a discussion of the analysis in Section 5. This section discusses the effectiveness of the study's novel proxy approach for matching non-simultaneous load and environmental measurements, particularly in light of environmental factors such as waves that are present at the real site but impossible to account for through the Delft3D model. Potential routes for further development of the method are explored in Section 6.

2. Settings

In this section, the deployment site of both the D10 and the Nortek Signature500 five-beam AD2CP is described, alongside the set-up of the turbine and configuration of the AD2CP for data collection. Furthermore, as some of the information gathered during this study is commercially sensitive, the following steps have been taken to anonymise the data: (i) where time series of AD2CP measurements are shown, the date at which the measurements are taken are not shown, and this is instead stated as the number of days since the start of the deployment; (ii) all power output values are non-dimensionalised with respect to the peak power generated throughout the whole deployment, i.e., all power output values fall in the range [0,1].

2.1. Site description

The measurements for this study were taken in the Fromveur Strait, a tidal channel separating the Isle of Ushant from the Molène archipelago off the west coast of Brittany, France (Figure 1a). Deemed to have the second greatest tidal stream potential along the French coast, a 4 km^2 restricted area situated towards the north-eastern end of the Strait was identified by the French Government for the development of tidal stream projects. Both the D10 and AD2CP were located within this region, where the channel is approximately 2 km wide and 55 m deep.

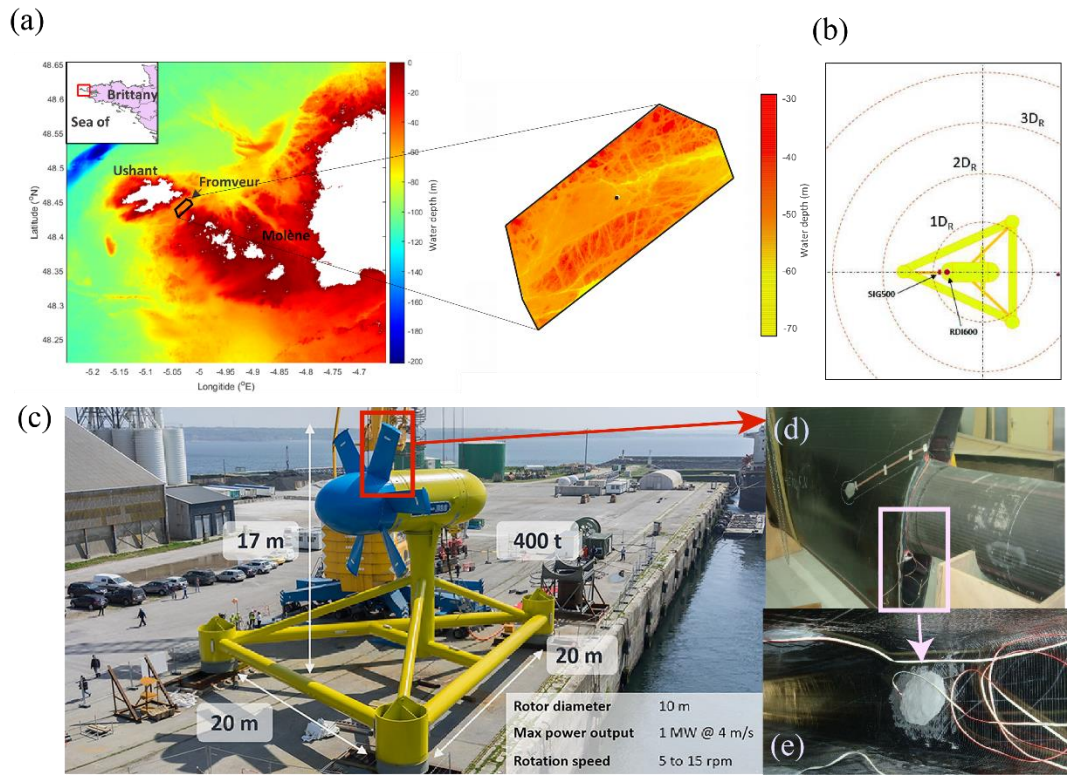

Figure 1. (a) Mean bathymetry surrounding the Ushant-Molène archipelago alongside area of focus for higher-resolution bathymetric mapping. Bathymetry data obtained from the European Marine Observation and Data Network. High resolution bathymetry of the Fromveur Strait (right-hand image) based on water level at lowest astronomical tide. Black dot represents location of D10. Bathymetry data obtained from the French Naval Oceanographic Centre SHOM ("Service Hydrographique et Océanographique de la Marine"); (b) schematic diagram of Sig500 location relative to D10; (c) dimensions of Sabella's D10 tidal stream turbine and its performance characteristics; (d) shin gauge mounted one on of device's blades (not used within this study); (e) three spar gauges bonded on the inside of the blade's spar. Original photos provided by Sabella.

The flow regime within the Strait is governed by semi-diurnal tides, where the principal flow direction is north-northeast with average velocity ellipses showing a clockwise rotation [16]. The deployment location is situated within the flood-dominated region of the Strait, although this dominance is only slight. Despite being situated within the shelter of the Isle of Ushant, significant wave heights in the area typically range between 1.5 - 3 m, with maximum wave heights liable to exceed 3.5 m when in storm conditions [17]. Bathymetric gradients alongside islands and rocks induce strong tidal flow acceleration within the Strait, resulting in peak tidal current magnitudes exceeding 3.8 ms^{-1} in spring tidal conditions. Such intense tide-induced flow results in a well-mixed water column with small variations in temperature and salinity between the surface level and the seabed, hence, no effects of stratification should be present in the analyses.

2.2. D10 tidal turbine

The Sabella D10 is a bottom-mounted, fully submerged tidal turbine comprising a single rotor with a horizontal axis and six fixed symmetrical blades (Figure 1b). The turbine has a diameter of 10 m and is designed for a power capacity approximately 0.5 – 1 MW in current speeds ranging between 3.0 - 4.0 ms^{-1}. The D10 was deployed in October 2018 for approximately one year and was equipped with numerous sensors located on the turbine itself, on the support frame and within its onshore power conversion and rectification station. For the purpose of this study, sensor measurements across a one-month period were used.

An in-built sensor on the generator measured the D10's instantaneous active power at a sample frequency of 1 Hz. Blade strain was obtained using three sensors located on the spar of one of the device's blades which recorded instantaneous values every 30 seconds (Figures 1c and 1d).

The D10 was running under the Maximum Power Point Tracking (MPPT) control mode, which continuously adjusts the rotational speed of the turbine to produce an optimal tip speed ratio. Thus, the turbine consistently runs at the optimal power coefficient, C_p.

2.3. AD2CP configuration

The AD2CP was a Nortek Signature500 device. During the study it was bottom mounted and its sensor head rested 1.0 m above the seabed. The instrument employs four slanted beams 25° from vertical, in addition to a fifth vertical beam. The recent implementation of a fifth vertical beam provides a direct and well-resolved calculation of the vertical velocity and surface elevation. The AD2CP was configured to continuously record velocities across 61 depth bins (spanning the entire water column) at 1 m spacing in XYZ_1Z_2 coordinates at a sampling rate of 1 Hz. The deployment period for the AD2CP spanned approximately seven months, providing more than sufficient record length to assess the variations in turbulence from varying harmonic lengthscales, including semi-diurnal and spring-neap profiles. A summary of device settings and deployment configurations is provided in Table 1.

Table 1. Sampling deployment summary for the Nortek Signature500 AD2CP at the Fromveur Strait.

Parameter	Value
Longitude (°E)	5.0336933
Latitude (°N)	48.447827
Deployment depth (m)	55
Height above seabed (m)	1.0
Measurement frequency (Hz)	1

Measurement interval (sec)	3600
Number of samples (N)	3600
Bin size (m)	1.0
Number of cells (N)	61
Blanking distance (m)	1.0

A simple stationarity test was carried out to determine the appropriate averaging period for the AD2CP data. A 30-minute time series of velocities from day 50 was taken at a single bin which was centred approximately 0.49 m above the D10 hub height. This sample corresponded to spring tide conditions where the flow was progressing from high to low water.

The flow speed was plotted with increasing sample time, ranging from one second to the full 30-minute sample. The calculated flow speed stabilises around 250 seconds. It was therefore decided that a time interval of five minutes (300 seconds) would be sufficient to burst average these data and estimate hydrodynamic parameters.

3. Research design and methods

3.1. Quantification of turbulence parameters from AD2CP

3.1.1. Surface wave decoupling

Accurate quantification of turbulence parameters remains a challenge in wavy aquatic environments - such as those found at in the Fromveur Strait - as wave motions tend to introduce bias in two forms: 1) the non-linearity of waves can result in the horizontal and vertical components of wave orbital velocities to migrate from exactly out of phase; and 2) in severe wave conditions, wave orbital motions can affect estimates of turbulent quantities. As eddies detected by the recording instrument are advected by both the mean current flow and wave orbital velocities, this means that to some extent wave kinematics influence the detected turbulent frequency spectra [18].

Taking the horizontal and vertical velocity components u and w, respectively, as an example, the shear stress in a wavy aquatic environment can be described as:

$$-\overline{u'w'} = -\overline{\tilde{u}\tilde{w}} - \overline{\tilde{u}w_t'} - \overline{u_t'\tilde{w}} - \overline{u_t'w_t'} \quad (1)$$

where n_t' = turbulent fluctuation components and $\tilde{n}$ = wave orbital velocity components for each velocity component. In this equation, $\overline{u_t'w_t'}$ represents the turbulent Reynolds shear stress within the current flow and the other three terms on the right-hand side describe motion due to waves. In an ideal environment, waves and turbulence are not

correlated, thus, if averaged over a period, the second and third terms on the right-hand side of (1) should disappear. However measured velocity components may not be completely out of phase due to non-linearity of waves or possible uncertainties in the sampling instrument's tilt, resulting in significant influence of wave stress ($-\overline{\tilde{u}\tilde{w}}$). Therefore, accurate estimation of TKE for the D10 performance analysis requires the removal of the influence of wave stresses.

Wave and turbulence decomposition was performed by applying a synchrosqueezed wavelet transform (SWT)-based method to the burst averaged AD2CP data [18]. This technique analyses the various frequencies embedded in the signal and separates the orbital wave and sinusoidal tidal behaviours from the chaotic turbulent frequencies and has been successfully applied to a potential tidal energy site [19]. Turbulence-only values derived from the SWT were then screened against acoustic backscatter amplitude and correlation values to remove excess noise. Amplitude and correlation values of the burst averaged AD2CP data less than 40 dB and 64 %, respectively, were removed from analysis and omitted from calculations.

3.1.2. Turbulence kinetic energy

TKE, typically measured as TKE density, k, is the most important metric to describe the strength of turbulence. TKE was calculated by employing a modification of the variance technique – a method well established in literature [20-22]. The calculation methodology extends the four-beam variance technique to determine TKE for a five-beam ADCP configuration [23], and is expressed as:

$$\mathrm{k} = \frac{1}{4\,sin^2\,\theta}\left(\overline{u_1'^2} + \overline{u_2'^2} + \overline{u_3'^2} + \overline{u_4'^2}\right) - 2\,(2\cos^2\theta - 2\sin^2)\,\theta u_5'^2 - (\cot\theta - 1)\phi_3\,(u_2'^2 - u_1'^2) \qquad (2)$$

where θ corresponds to the beam inclination angle (25° in this instance), ϕ_3 relates to the AD2CP's mean pitch, and the $u_i'^2$ refer to the along-beam velocity fluctuations with the subscript specifying the beam number. For the purpose of this study, we use a single depth-averaged value of TKE across the D10's rotor diameter for each five-minute sample period unless stated otherwise.

This technique corrects for tilts when calculating TKE. As with all implementations of the variance method, this method relies on making two critical assumptions regarding the flow behaviour across the AD2CP sample plane. Specifically, it is assumed that second-order statistics are homogenous across all beams, and that such statistics do not vary significantly across the time-averaging period.

3.2. D10 performance metrics

Consistent with the sample period used to estimate hydrodynamic characteristics, the D10's active power and blade strain were averaged across a period of five minutes, excluding periods when the turbine was parked. Active power measurements were sampled at 1 Hz, but as stated in section 2.3, strain is sampled once every 30 s. A single variance calculation for strain therefore uses ten instantaneous measurements.

3.3. Establishment of environmental proxy

3.3.1. Correspondence of environmental conditions with modelled water depth

Difficulties with the current sensor on the D10 meant velocity data at the turbine's location was not obtained during the turbine's deployment. Consequently, a direct relationship between the environmental data (i.e. velocity) from the AD2CP and the D10 performance metrics could not be determined. This is the technical difficulty that motivated the introduction of the proxy mentioned within Section 2. The specific proxy used for current speed was the rate of change of surface water level (dz/dt) in a computational model of the deployment site. This allowed populations of non-simultaneous measurements of turbulence and loads from similar tidal current conditions, accounting for spring-neap variation, to be compared with one another.

Tidal elevation was modelled using Delft3D, with a simple forward-difference scheme used to determine an average dz/dt for each five-minute period. The model employed bathymetry from GEBCO ("General Bathymetric Chart of the Oceans") and was forced by uniform water level boundaries using astronomical tidal constituents. The tidal elevation model was validated against AD2CP pressure data obtained across a one-month period, producing an R value of 0.9901 (see Appendix A). The use of dz/dt as an environmental proxy for tidal current conditions was validated using current speed measurements obtained by the AD2CP across the same one-month period, producing an R value of 0.9297 (see Appendix A).

Although dz/dt is clearly a satisfactory proxy for current speed, differences between turbulent structures generated on accelerating and decelerating phases of the tidal cycle mean that analyses of turbulence parameters from only comparable velocity measurements may not be entirely sufficient. Turbulence and velocity do not necessarily respond at the same rate: thus, turbulence parameters measured on accelerating phases of the tidal cycle will differ from those measured on decelerating phases. The deceleration

phase typically contains larger coherent boundary layer structures which contribute more to non-uniformity as the flow decelerates [24]. Thus, although velocities and TKE may be comparable, it may be expected that loading on a tidal turbine would fluctuate more across a decelerating phase compared to a steady increase in load when the flow is accelerating. To assess this further, the calculated rates of change in tidal elevation were categorised into accelerating and decelerating phases of the flood-ebb tidal cycle.

3.3.2. Associations of D10 performance and turbulence characteristics

The five-minute average estimates of D10 performance metrics and turbulence parameters were sorted into bins using the rate of change of tidal elevation for both the AD2CP and D10 deployment periods from the Delft3D data. This allows us to categorise similar flow conditions together, regardless of their position in the spring-neap cycle; thus, for instance, peak flow at a neap tide is regarded as part of the same population as a mid-tide flow at a spring.

Once determined, these bins were split further to introduce accelerating and decelerating periods of the tidal cycle. The "slack" category was not split further as it was assumed that turbulent characteristics across both accelerating and decelerating periods would be relatively settled and would show no significant difference. Thus, 13 bins were defined into which the D10 performance data and turbulence parameters were classified. These bins are shown in Table 2.

Table 2. Bin classifications employed to establish relationship between environmental conditions for D10 performance parameters and AD2CP turbulence quantifications. Correspondence between tidal elevation rate and recorded AD2CP velocity measurements for each bin are shown. n represents the rate of tidal elevation change for each measurement. Rate of change was determined as meters per hour. Mean AD2CP flow speed for each bin is shown. Flood/ebb flows were determined by a positive/negative rate of change, respectively, with the flow split into accelerating and decelerating components dependant on the corresponding surface water height.

Bin classification		**dz/dt (mh^{-1})**	**Mean current (ms^{-1})**
Accelerating flow	Fastest flood	1.25 < n <= 1.65	2.8881
	High flood	0.75 < n <= 1.25	2.2562
	Low flood	0.25 < n <= 0.75	0.8784
	Low ebb	-0.25 > n >= -0.75	0.8759
	High ebb	-0.75 > n >= -1.25	1.9540
	Fastest ebb	-1.25 > n >= -1.65	2.6556
Slack	Slack	0.25 >= n >= -0.25	0.5115
Decelerating flow	Fastest flood	1.25 < n <= 1.65	2.6017
	High flood	0.75 < n <= 1.25	1.9758
	Low flood	0.25 < n <= 0.75	1.2385
	Low ebb	-0.25 > n >= -0.75	1.3996
	High ebb	-0.75 > n >= -1.25	2.1301

	Fastest ebb	-1.25 > n >= -1.65	2.6857

4. Results

4.1. Hydrodynamic measurements of the Fromveur Strait

A period between Day 46 – Day 55 demonstrates typical hydrodynamics within the Fromveur Strait during the transition from neap to spring tide (Figure 2). Differences in flow speed throughout the water column can be seen in the contour plots of depth-varying parameters, with maximum flows of 4.60 ms^{-1} in spring conditions (Days 53-54) and 2.55 ms^{-1} in neap conditions (Days 47-48). Larger TKE values parallel the increase in flow speed from neap to spring tides, with depth-averaged TKE increasing from 0.0149 m^2s^{-2} to 0.0247 m^2s^{-2} within this period.

A prominent turbulent structure is visible in Figure 2c, spanning most of the progression from neap to spring (Day 46-52). This structure is associated with increases in TKE of approximately 0.1 m^2s^{-2} and appears to oscillate vertically around a depth of 30 m, concurrent with changes in surface height. It is difficult to attribute this feature to a particular source; however, since the vertical oscillations closely track the surface height change, this turbulent structure is conjectured to be an artefact within the AD2CP signal. The specific mechanism that could generate this return was not determined. As the feature appears on both floods and ebbs, we discounted potential explanations relating it to the device wake.

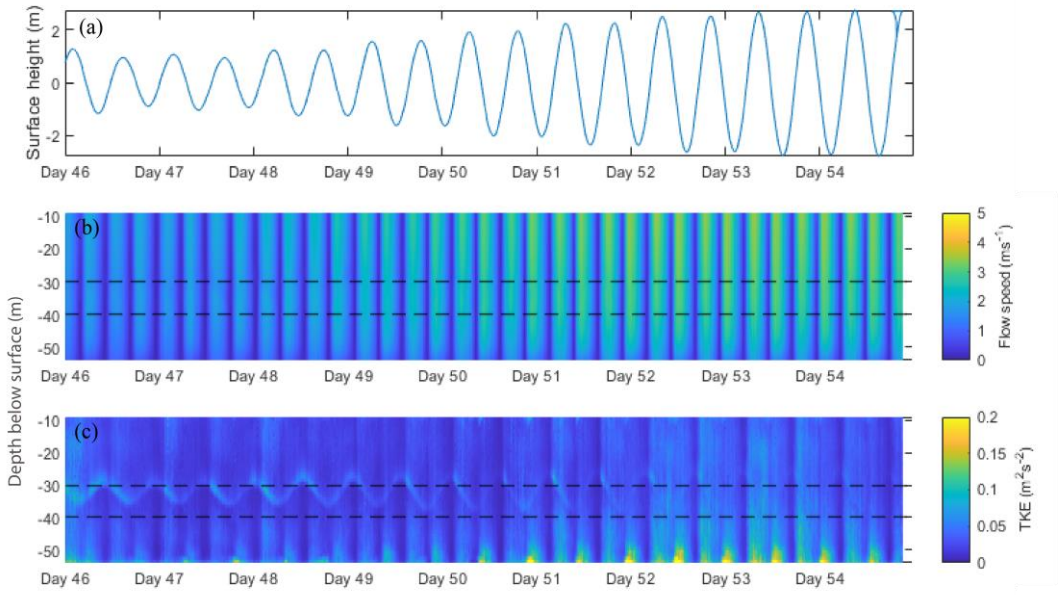

Figure 2. Contour plots of depth-varying measured and calculated hydrodynamic characteristics of the Fromveur Strait from neap to spring tide, demonstrating (a) change in surface water level height, (b) mean velocity measured across each AD2CP bin, (c) calculated TKE. The area of interest is established by the black dotted lines, representing the rotor spinning area across 30-40 m depth.

Mean vertical profiles of flow speed and TKE across flood and ebb tides are shown in Figure 3, further sub-classified into spring and neap. Flood velocities are typically slightly larger than ebb velocities across all depths, but flood and ebb profiles showing no significant asymmetry in depth distribution for all the recorded parameters across the water column, regardless of spring or neap conditions. A small local decrease in ebb velocity is visible between 30 – 35 m; a similar local increase of greater magnitude is also visible in the TKE distribution. This is consistent with the turbulent structure seen in Figure 2c. For both flood and ebb flows, TKE increases towards the bed with the presence of a boundary structure apparent between 50 – 55 m where TKE reaches as high as approximately 0.09 m^2s^{-2} in spring flood conditions.

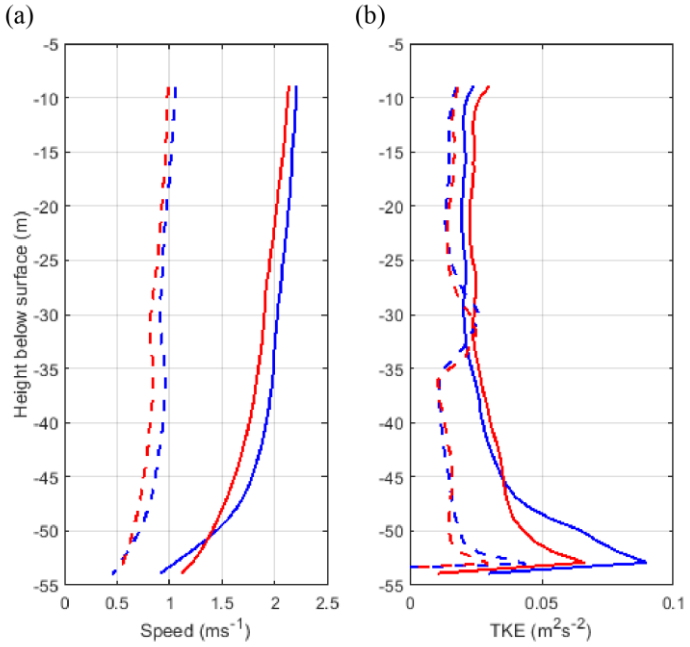

Figure 3. Vertical profiles of (a) mean current speed and (b) TKE from Fromveur Strait. Profiles are split into flood (blue) and ebb (red) and spring (solid) and neap (dashed) lines.

4.1.1. TKE profiles across study area

Flow characteristics across two representative tidal cycles as measured by the AD2CP are shown in Figures 4a and 4b, taken from deployment days 49-50. These measurements

show values from a depth-average across the rotor diameter of the D10. Although TKE is in general depth dependent, previous investigations in the literature show that such values do not tend to vary significantly across the portion of the water column encompassed by the rotors of bottom-mounted devices of similar size to the D10 [19]. This is consistent with the TKE profiles observed in Figure 4, so we are confident that a single depth-average value for TKE is appropriate.

From the time series (Figures 4a and 4b), it is clear that TKE measurements are well correlated with the speed of the current, showing the same pattern of rapid acceleration to peaks of approximately 0.06 m^2s^{-2} as the flow accelerates, and then more gradual decreases as the flow decelerates. During slack water periods, turbulence levels tend to remain around 0.02 m^2s^{-2}.

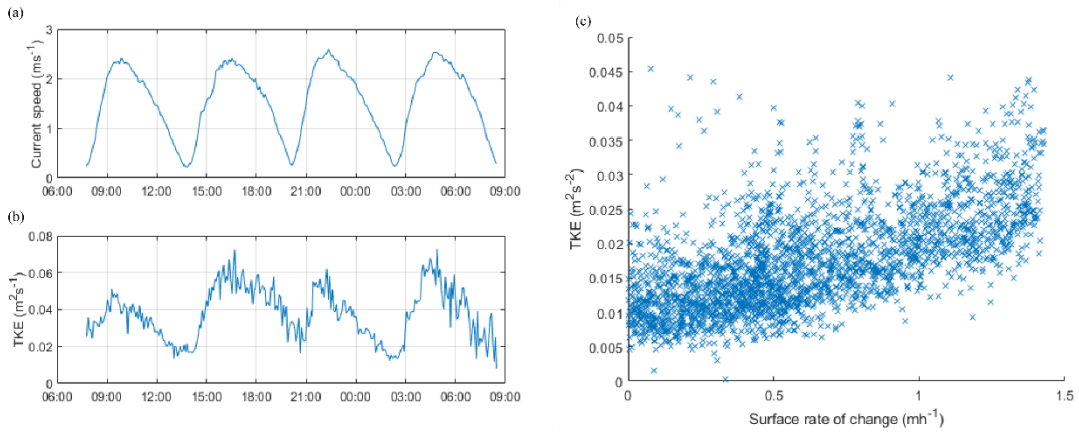

Figure 4. (a) Time-series of flow speed depth-averaged across the rotor diameter (30 - 40 m depth); (b) time-series of TKE for corresponding current speeds. Both datasets are averaged across five-minute periods throughout two full tidal cycles; (c) depth averaged TKE plotted against $\boldsymbol{dz/dt}$.

The relation between TKE as measured by the AD2CP and magnitude of dz/dt as predicted by the Delft3D model across a one-month period is shown in Figure 4c. Outcomes of a linear regression analysis indicate a significant relationship between dz/dt and TKE ($R^2 = 0.076$, $F = 15.6$, $p < 0.05$). Larger values of TKE are seen for higher dz/dt values, signifying larger turbulence values for higher current flows. Approximately, TKE increases from 0.01 - 0.025 m^2s^{-2} as dz/dt increases from approximately 0 - 1.5 mh^{-1}. These measurements, particularly across the higher velocities, are similar to results reported at other prospective tidal sites for the increase in TKE magnitude with faster current flows [19], [25-26].

Histograms of TKE across each of the 13 dz/dt bins used within this study are shown in Figure 5. Visualising the TKE in this way, the same tendencies as indicated in Figure 2c can be seen in greater detail, with population-mean TKE values exceeding 0.03 m^2s^{-2} for the fastest flow profiles and decreasing to approximately 0.01 m^2s^{-2} for the lower flow and slack profiles.

Ebb flows generally exhibit higher mean turbulence than floods. Furthermore, the distributions shown in Figure 5 indicate that although flood tides exhibit increased turbulence on accelerating flows, ebb tides exhibit increased turbulence on decelerating flows - the influence of an flow acceleration and deceleration is discussed further in Section 4.1.2. In this instance, the tendency for ebb flows to have not only a higher TKE, but also a greater chance of more extreme departures from the mean (average standard deviation, σ, of 0.0147 m^2s^{-2} compared to σ of 0.0123 m^2s^{-2} for floods) means that the difference between floods and ebbs regarding extreme TKE values is larger than a simple comparison of the means would suggest.

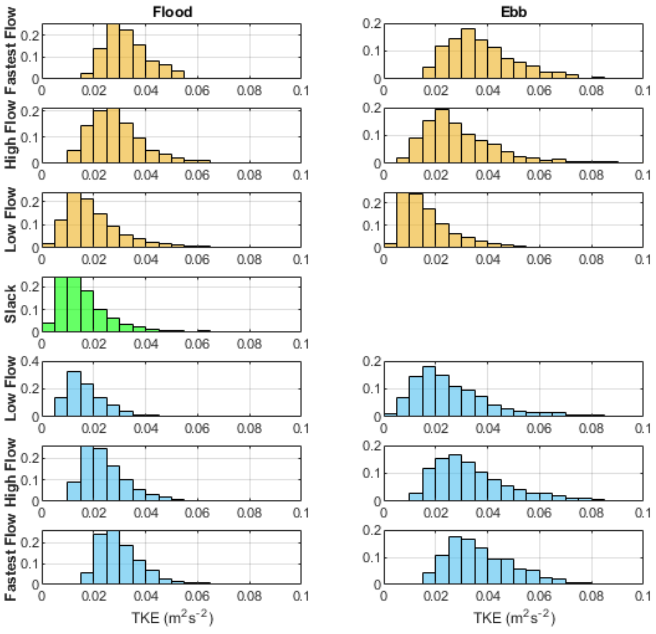

Figure 5. Normalised probability distributions of TKE across the 13 bins representing the tidal cycle across both flood and ebb flows. Orange plots represent an accelerating tidal flow, green plots represent slack tide and blue plots represent a decelerating tidal flow.

4.1.2. Effect of accelerating and decelerating flows on TKE

Referring back to Figure 4b, it is clear that TKE increases rapidly towards its peak during periods of accelerating flow. When the flow is decelerating towards slack, a more gradual

decrease in TKE is seen, coupled with larger fluctuations. This parallels the asymmetry in acceleration and deceleration of mean current speed that is found within this section of the Fromveur Strait, where the flow accelerates from slack to peak speed in approximately two hours whereas deceleration of the flow to slack occurs over three to four hours.

Mean TKE depth-profiles across the D10's rotor diameter were plotted across three tidal cycles for both spring and neap cycles (Figure 6). Flood flows typically exhibit higher-than-mean TKE values for accelerating flows, whereas ebb flows are more variable but broadly tend to larger TKE values across decelerating tides. This is in line with what was seen for the average across all depths in Figure 3. Larger differences between accelerating and decelerating TKE values are seen within upper water column for all profiles, but deeper in the water column (particularly below 36 m for the neap profiles) the effect of flow acceleration is less pronounced. Three of the four plots on Figure 6 (i.e., spring ebbs and neap ebbs and foods) show a feature whereby the accelerating and decelerating TKE profiles changing about the mean between depths of 31 m to 37 m. This is the same turbulence structure observed across the mid-water column in Figure 2c.

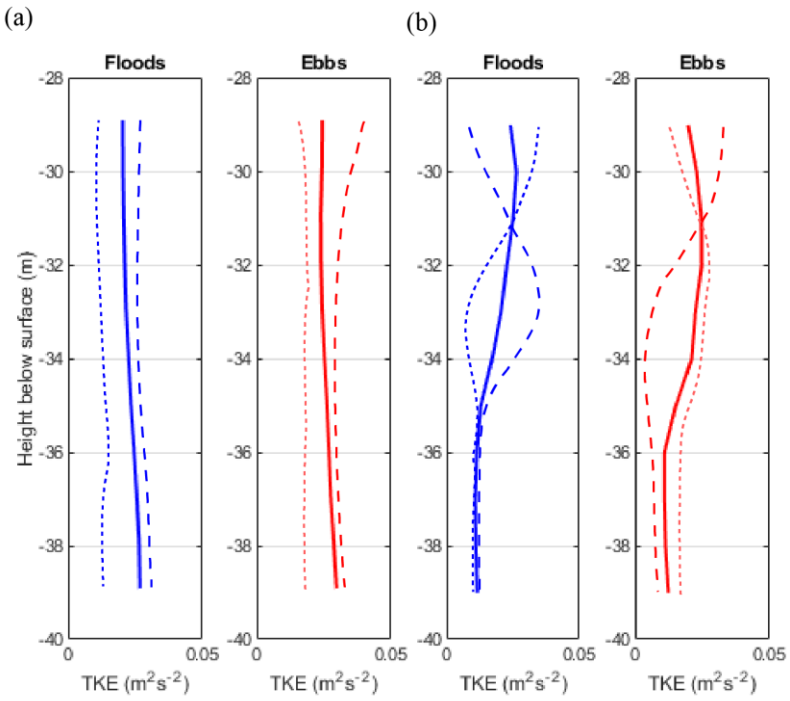

Figure 6. Depth profiles of mean TKE across the diameter of the D10's rotor, averaged across three (a) spring tides and (b) neap tides. Mean profiles are shown as solid lines. Dashed lines represent accelerating tides and dotted lines represent decelerating tides.

The influence of an accelerating and decelerating flow on depth-averaged TKE was evaluated using a two-sample Kolmogorov-Smirnoff statistical test. On this basis the null hypothesis, H_0, can be rejected at the 5% significance level for all tidal cycle classifications except the low ebb bin. In other words, we are 95% confident that depth-averaged TKE is statistically different in accelerating and decelerating flows, as well as between floods and ebbs or springs and neaps.

When evaluating TKE distributions within flood flows, higher magnitudes are present for accelerating flows. It is worth recalling that mean AD2CP velocities corresponding to acceleration periods of the flood flow demonstrate higher values when compared to periods of deceleration, particularly across the two fastest bins (Table 2). This suggests that the flow is channelled towards the AD2CP and D10 devices within these periods of the tidal cycle, inducing larger velocity measurements as a result. These larger current speeds would be associated with greater TKE magnitude. In turn, this suggests that the apparent influence of the accelerating and decelerating flows may in fact be due to differences in velocity measurements within each dz/dt bin.

4.2. Effect of TKE on the variability of D10 performance metrics

4.2.1. Active power

As expected, a broad trend of increased load variability with increased TKE is seen in Figure 7a, with larger spreads of the active power distributions evident within the fastest flow and high flow bins for both flood and ebb tides. Spreads greater that 0.11 (cf. Section 2 for details of power scaling) were seen across all fastest flow populations. The largest population standard deviation of 0.19 was seen across the high accelerating flood flow - a value approximately 0.03 greater than fastest accelerating floods - with the lowest decelerating floods and ebbs producing $\sigma = 0.02$. Flood flows produce larger variations in active power across all dz/dt bins than the corresponding ebbs.

The quantile-quantile (QQ) plots in Figure 7 show the relationship between the variability of active power (characterised as the standard deviation of active power for each five-minute averaging period) against TKE. All plots show a relatively linear relationship, establishing a roughly linear dependence between TKE and active power variability, even within each dz/dt bin. Some non-linearity is evident at the highest values of TKE across all plots as distributions deviate from the 1:1 line; this trend is particularly evident across

decelerating tides, where the non-linearity suggests that for extreme TKE values power variability increases non-linearly.

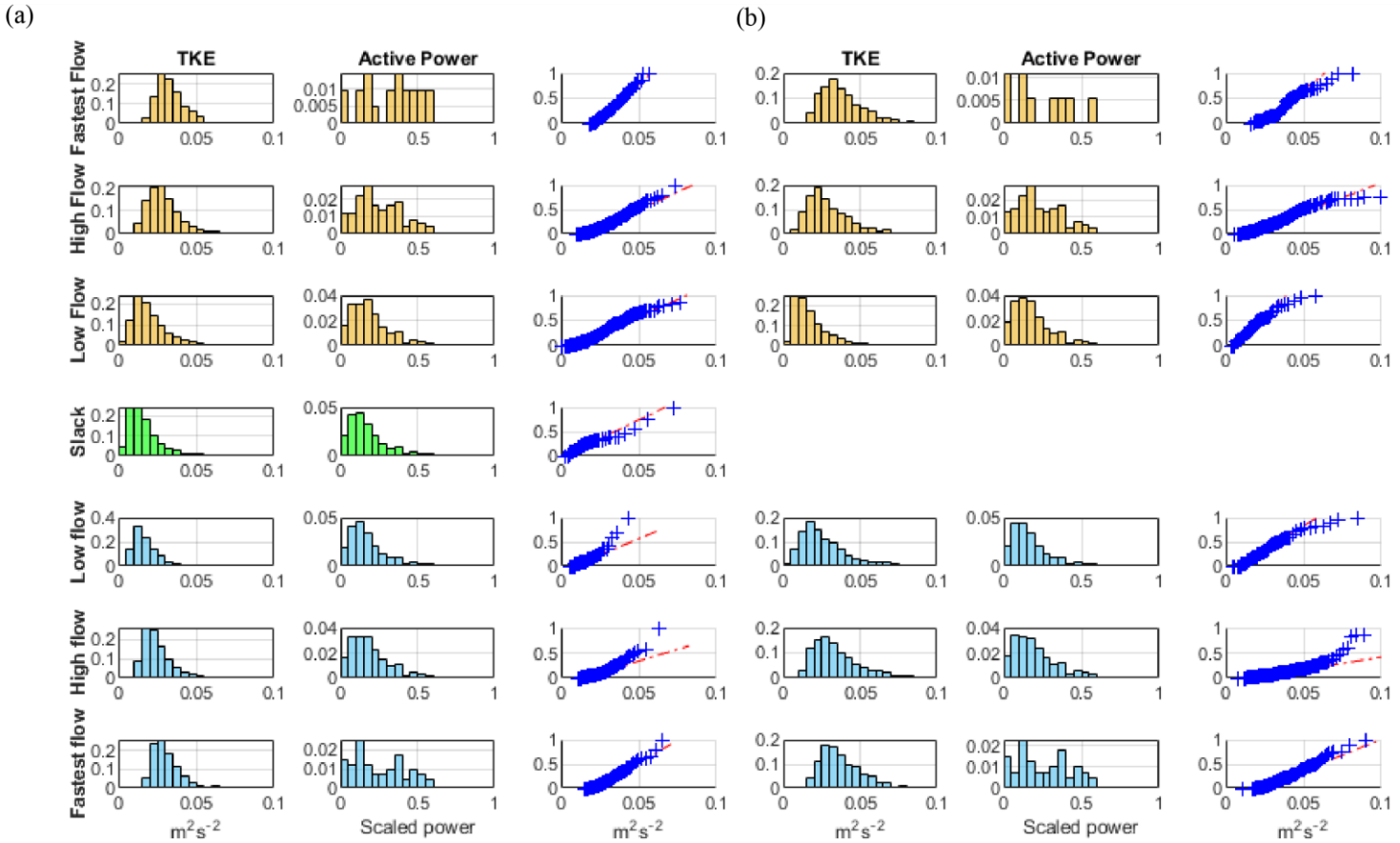

Figure 7. Normalised probability distributions of the D10's active power against TKE for (a) flood and (b) ebb classification bins and quantile-quantile plots for each $\boldsymbol{dz/dt}$ bin, plotting TKE against the standard deviation of active power. In histograms, orange plots demonstrate an accelerating flow, green demonstrates slack tide and blue plots demonstrate a decelerating tide. In QQ plots, red dashed line indicates the theoretical corresponding quantile values for both distributions. The slack period was not split into flood and ebbs and is instead provided as its own classification.

4.2.2. Blade strain

Blade strain against dz/dt was plotted for each of the strain sensors described in section 2.2; data two of the gauges were disregarded for further investigation due to excessively noisy measurements. For the third gauge, the expected tendency for increased strain variance as dz/dt increases is clear (see Appendix B), although a large proportion of the data cluster towards around near-zero values of variance. This tendency towards lower variance is reflected in the relatively low calculated R value of 0.33.

Histograms depicting the population distributions of blade strain variance for each dz/dt bin, alongside corresponding TKE populations, nonetheless depict a tendency for the variance in blade strain to increase as the TKE increases (Figure 8). Across the fastest flows (for dz/dt values in the range 1.25 - 1.65 mh^{-1}), variance in microstrain typically reaches maximum values between 400-500, although the distributions remain skewed towards lower variance values (< 100). Strain variance for dz/dt values in the range 0.75 - 1.25 mh^{-1} typically demonstrate maximum values up to 300, whereas most of the distribution of strain variance within the lower and slack flows are within 0 - 200.

A relatively consistent increase in the range of strain variance from slack to faster flows is seen, with particular prominence across ebb flows. Peaks within the majority distributions do not vary significantly between dz/dt magnitudes, with a consistent positive skewness across all plots, conjectured to be a result of the relatively low sampling rate of strain measurements which variance was calculated from. The distributions in strain variance across all populations are fat-tailed, with extreme values in excess of 250. Nevertheless, the 50 - 75 bin is consistently the modal or near-modal value of strain variance across both flood and ebb tides. The accelerating or decelerating nature of the flow makes no significant difference in blade strain variance according to the Kolmogorov-Smirnoff test.

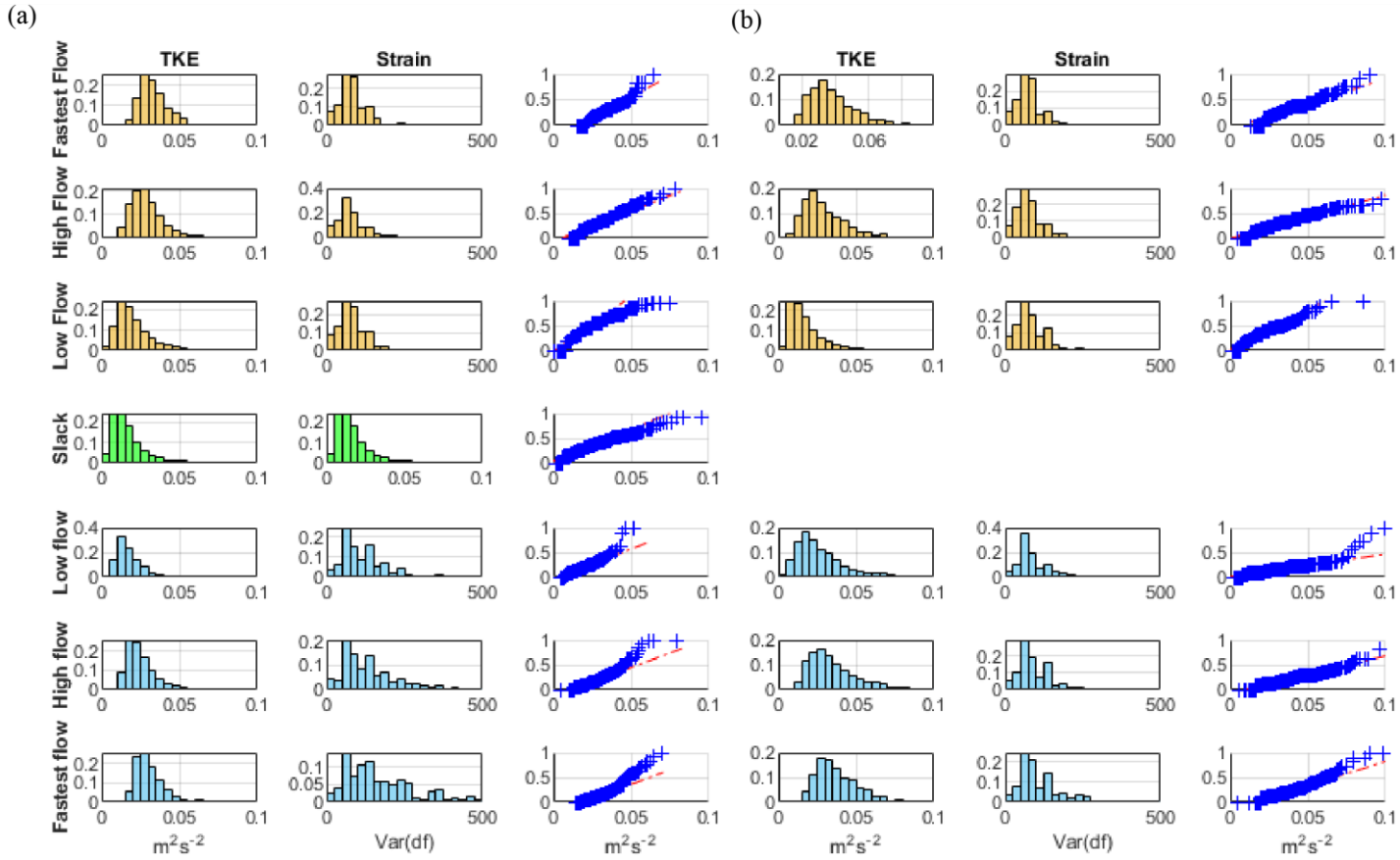

Figure 8. Normalised probability distributions of TKE across (a) flood and (b) ebb cycles against strain data variance for Gauge 3 and quantile-quantile plots for each $\boldsymbol{dz/dt}$ bin, plotting TKE against the standard deviation of active power. In histograms, orange plots represent accelerating periods, green represents slack tide and blue represents decelerating periods of the tidal cycle. In QQ plots, red dashed line indicates the theoretical corresponding quantile values for both distributions. The slack period was not split into flood and ebbs and is instead provided as its own classification.

5. Discussion

Knowledge of the nature of turbulence in tidal channels, and how it affects the performance of tidal turbines, is critical for comprehensive understanding of how unsteady hydrodynamics affect tidal stream devices. Obtaining simultaneous measurements of environmental data and tidal turbine performance metrics is often a difficult task, owing to expensive deployment operations and inconsistencies in hydrodynamics across deployment sites.

In this paper, we considered a data set from the full-scale D10 tidal turbine deployed within the Fromveur Strait where environmental and performance data were not measured simultaneously. By employing a Delft3D proxy, a comparison can be carried out between turbulence measurements and performance data that are drawn from similar conditions. In general, findings demonstrate that larger turbulence values and more variable performance data are strongly associated via the proxy, despite being measured at a different time. TKE magnitudes typically agreed with those recorded at other tidal energy sites, ranging mostly between 0.01 m^2s^{-2} and 0.03 m^2s^{-2} [24-26] for both flood and ebb flows. As the deployment site for both the AD2CP and D10 was located within the flood-dominated section of the Strait, consistently higher TKE values across the ebb profile suggest an asymmetric influence of the surrounding bathymetry and surface roughness on the development of turbulent structures. Although the bathymetric map suggests the upstream seabed is similar on both flood and ebb (Figure 1) it is possible that the presence of undetected boulders may have resulted in the formation of larger turbulence structures in the direction of the ebb flow – this is, however, unlikely with the level of resolution in the bathymetric data used. An alternative hypothesis is that the ebb flow experiences long-persistence high turbulence features from a site further upstream, or that turbulence in flows from the northeast is enhanced by a greater degree due to the more rapid decrease in water depth for flows coming from that direction. Investigation into both hypotheses would require extensive hydrodynamic research across the Fromveur Strait.

Analysis of active power measurements alongside TKE values for each dz/dt bin suggest that the variability of turbine power production is approximately linearly related to TKE levels. It was shown in results presented in Figure 7a that larger TKE values increased the variability of active power with a roughly linear relationship. This is consistent with previous studies that demonstrated increasing fluctuations in rotor torque and thrust with an increase in turbulence metrics [9-10]. This is the case in general for an

increasing current flow from slack to peak velocities, independent of spring-neap cycles. In addition to this general tendency it was observed that flooding tides within the Strait demonstrate larger overall variance in active power compared to ebbing tides with similar current magnitudes, with load measurements within the high accelerating flood bin producing the largest variance of $\sigma = 0.19$ (scaled).

This observation is also borne out for most dz/dt bins on the ebbing tide, with the exception of the fastest ebbs. It is uncertain as to why this is the case, but the conjecture is that it is a result of the technique used to classify the bins within this study. Although the dz/dt proxy is well correlated with faster current flows as measured by the AD2CP ($R = 0.9297$), bin widths of ~0.25 mh^{-1} may have introduced errors. For example, the minimum current speed recorded by the AD2CP within dz/dt values in the range 0.25 - 0.75 mh^{-1} was 0.14 ms^{-1}, which is similar to the minimum current speed of 0.11 ms^{-1} classified in dz/dt values in the range 0 - 0.25 mh^{-1}. If similar overlap is also present during the time that performance data was measured, then the proxy method may be comparing environmental and load measurements from dissimilar flow conditions in the low-magnitude dz/dt bins. Narrower ranges for the dz/dt bins might address this issue where more data is available, but this was not practical in the current study where some bins already had relatively few data points.

Investigating the relationship between blade load levels and turbulence also shows a clear relation between blade strain variance and TKE, as shown in Figure 8. These findings suggest that larger strain variance is strongly associated with higher levels of TKE, and can thus be understood to be a consequence of the fluctuating angles in the velocity field encountered by each blade [4]. Typical peak strain variance in excess of 400 was recorded across dz/dt values in the range of 1.25 - 1.75 mh^{-1} as TKE values averaged 0.036 m^2s^{-2}, whereas strain variance limited to ~200 was evident across lower dz/dt classifications, where TKE reached a mean of 0.018 m^2s^{-2}. In other reports, instantaneous measures of blade bending root moment calculated by computational fluid dynamic modelling demonstrates variability in excess of 2000 kNm for turbulence intensities of 12% across velocities of 3 ms^{-1} - an appreciable increase from 500 kNm variability across flows containing 0 - 5% turbulence intensities for same velocities [29]; this proportionality is consistent with what we observe in the current study. Additional laboratory-based studies (approximately $1/30^{th}$ scale) have also demonstrated distinct sensitivity of mean thrust to

variation in turbulence intensities between 3% and 25% [9] [30]. However, these studies do not report the inlet turbulence scales, which makes scaling these results to full-scale challenging. Although this study did examine the effect of turbulence on whole-rotor thrust, there is still a lack of studies investigating TKE's relationship with blade load variance, which means a direct comparison and evaluation of the current study of blade strain variance with similar studies on other tidal devices and deployment sites is essentially unobtainable at present.

As noted, when matching populations of TKE and performance or load variance through the proxy, there is a clear correlation between stronger turbulence and greater variability. The QQ plots of figures 7 & 8 show that, in addition to this population-level agreement, non-simultaneous measurements also show that the TKE and load variability within each population are distributed similarly. In other words, the method shows that not only can a population of TKE values taken from a time of known mean flow properties broadly predict the median load variance for all other similar times, but that the shape of the load variance distribution (except for its extreme high values) can also be expected to match the shape of the TKE distribution.

The technique used within this study to classify dz/dt into accelerating and decelerating flow periods may introduce classification errors into the analyses, particularly around the periods of fastest flows when the water level is nearing the referenced mean surface height (i.e., the boundary between accelerating and decelerating categories). In this instance, statistical tests such as ANCOVA may be better applied to distinguish accurate accelerating and decelerating information, although the lack of in-situ velocity data for the D10 deployment limits reliability of such tests. In addition, a form of bias may have been introduced when separating depth-averaged TKE into accelerating and decelerating components due to the artefact left within the AD2CP signal across 29 - 37 m depth (see the discussion in section 4.1 and section 4.1.2).

The influence of surface gravity waves was removed from this analysis using the SWT technique to allow more accurate estimations of turbulence characteristics and its effect on the efficiency of the D10. Nevertheless, significant surface gravity waves which are often found at highly energetic tidal energy sites introduce further loading on tidal turbines. Although this influence decreases with depth, surface wave activity has the potential to dominate turbulent fluctuations in the upper half of moderately deep (~40 m)

water columns, with previous studies noting considerable fluctuations in turbine performance characteristics due to the strong influence additional loading from surface wave activity [20] [22]. It could be argued that the overall magnitude and period of load experienced by a turbine are more valuable when predicting performance fluctuations and subsequent fatigue cycles, but the ability to determine whether turbulence or surface waves is driving fluctuations in turbine performance and loads is necessary, particularly in the interest of predicting tidal fatigue sources and patterns in varying aquatic environments.

It should also be noted that the dz/dt proxy implemented within this study cannot provide information about the wave environment. Thus, if waves have a dominating influence on the load variance within the Fromveur Strait, then the current approach is less suitable. This is particularly pertinent considering the phenomenon observed within the TKE depth contour plots (Figure 2c). As this feature appears to track the surface height in time, it is potentially associated with wave activity, and thus a different implementation of the SWT may alter the influence this feature has on the overall results.

6. Conclusion

The results presented here show the performance of the D10 tidal turbine (1 MW) subject to highly turbulent and variable flow conditions that are associated with its deployment site used in the Fromveur Strait. Despite the lack of velocity data across the deployment period of the D10, it was possible to obtain statistically comparable mean flow speed and mean TKE data corresponding to the performance data by using a Delft3D model of water depth, which appeared to be a sufficient proxy for the required period. This method should be applicable to other tidal stream energy deployment sites, allowing changes in device performance and loads in response to different TKE conditions to be anticipated even where simultaneous measurements are not available.

The proxy is less suitable if the influences of wave behaviour is expected to dominate over the effects of turbulence. Comparison of active power variance and TKE as paired by the Delft3D proxy shows good correlation between high TKE measurements and high standard deviations of active power. Assessment of blade strain variance and TKE also demonstrates that higher variability in structural loading coincides with larger TKE, although the confidence level of this relationship is lower than the one between TKE and power. Examination of these data show that the distribution in strain variance is fat-tailed,

with extreme values much higher than the centre of the population would suggest. This is consistent across all proxy categories. The reason behind this is unclear, although in light of the need to discard measurements from two of the three strain gauges due to excessive noise, errors with the instrument may be a possibility..

Evaluation of the variability of active power and blade variance across accelerating and decelerating tidal flows showed mixed results. Significant differences in active power variability across accelerating and decelerating flows were found, with larger variability seen in accelerating tides despite larger TKE recorded across decelerating tides. Comparison of strain variance showed no significant difference across accelerating and decelerating tides and instead demonstrated high blade variance across all proxy classifications. Whether these results reflect the dynamics of the D10 or an artefact of the AD2CP setup is unclear. A longer dataset would be required to resolve this question.

Despite the lack of simultaneous environmental data and tidal turbine performance metrics, comparison with data from numerical and laboratory-scale investigations alongside hydrodynamic measurements collected at other tidal energy sites suggests that the relationship established between turbulence and turbine behaviour by the proxy model can be treated as reliable [19][25-26]. Further work is required to determine whether similar conclusions are drawn from comparisons of TKE and load variability, specifically blade variance, for full-scale devices deployed at other tidal sites. It should be borne in mind that the presence of the turbine itself will also influence turbulence measurements and, as such, future investigations may consider also incorporating this effect into the proxy model.

Acknowledgements

This study was performed in collaboration with the MONITOR project, which is co-financed by the European Regional Development Fund through the Interreg Atlantic Area Programme (EAPA_333/2016). AD2CP data were kindly provided by the project and performance data of the D10 turbine were kindly provided by SABELLA S.A., who are working in collaboration with the MONITOR project. André Pacheco also acknowledges the support of the Portuguese Foundation for Science and Technology (FCT) through the grant UID/MAR/00350/2020 attributed to CIMA, University of Algarve.

Appendix A

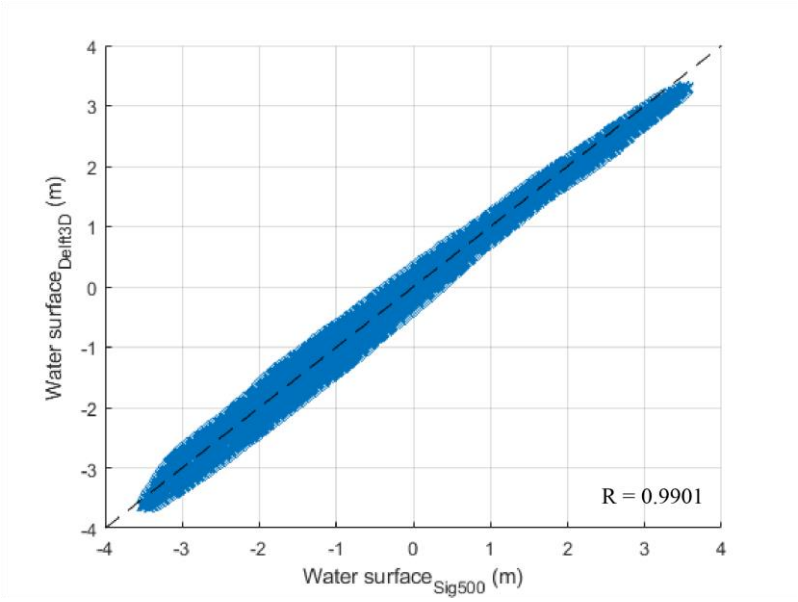

Figure A1. Comparison of modelled surface water elevation from Deflt3D and measured pressure data from the AD2CP across a one-month period. Measurements from both the model and AD2CP are instantaneous points five minutes. The dashed black line represents a y = x relationship.

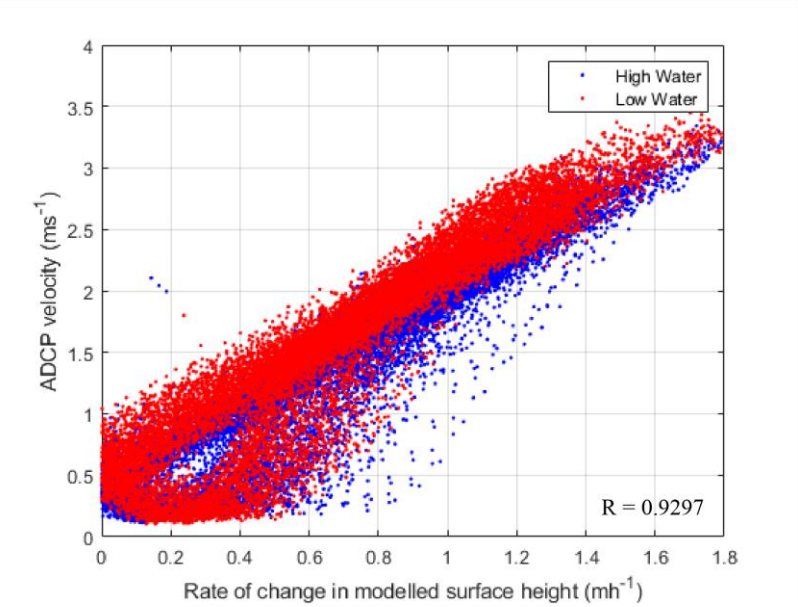

Figure A2. Association of the rate of change of surface water height calculated using the Delft3D model to the mean velocity obtained from the AD2CP measured across the theoretical height of the D10's rotor diameter (30 - 40 m). Measurements taken as five-minute averages across a one-month period. Blue dots represent measurements associated with "high water" - when the surface level exceeded the mean surface elevation for the AD2CP deployment - and red dots represent measurements associated with "low water" - when the surface height was below the mean surface elevation.

Appendix B

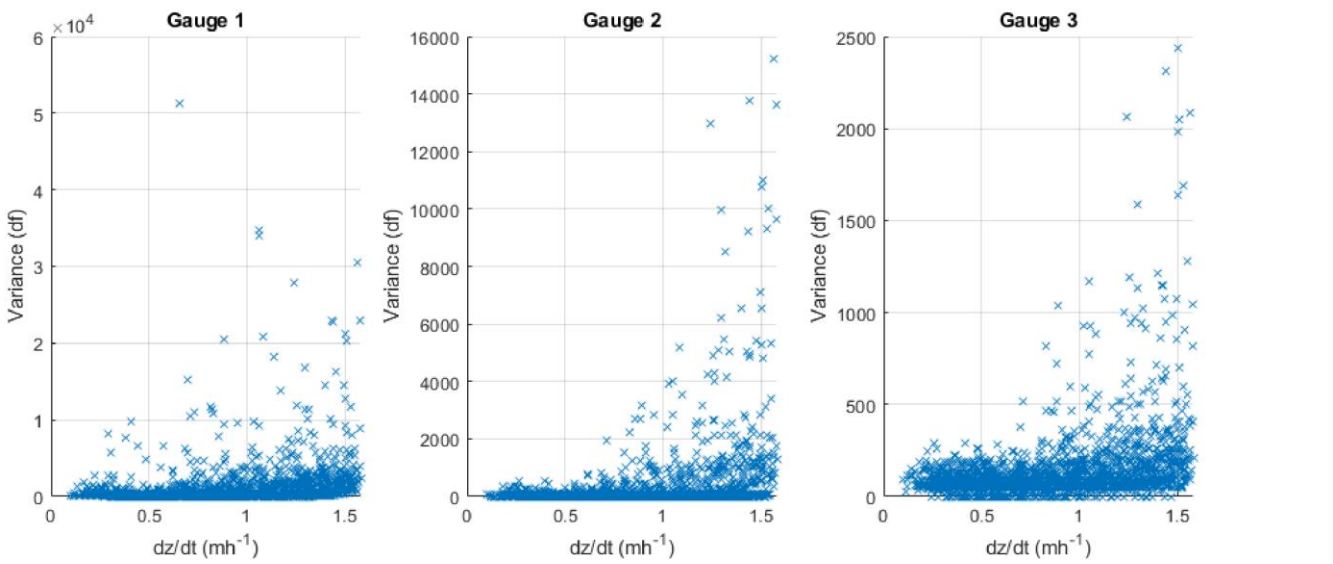

Figure B1. Distributions of blade strain variance against dz/dt for gauge 1, gauge 2 and gauge 3. Strain variance is presented as the variance in deformation. Gauges 1 and 2 were discarded due a to high proportion of noise measurements.

References

[1] Savidge, G., Ainsworth, D., Bearhop, S., Christen, N., Elsaesser, B., Fortune, F., Inger, R., Kennedy, R., McRobert, A., Plummer, K.E. and Pritchard, D.W., 2014. Strangford Lough and the SeaGen tidal turbine. In Marine renewable energy technology and environmental interactions (pp. 153-172). Springer, Dordrecht (doi:10.1007/978-94-017-8002-5_12)

[2] Simec Atlantis Energy, 2021. *Tidal Stream Projects, Meygen.* Available online: https://simecatlantis.com/projects/meygen/ [accessed 22 June 2021].

[3] Orbital Marine Power, 2021. *Orbital 2MW O2.* Available online: https://orbitalmarine.com/o2/ [accessed 22 June 2021].

[4] Milne, I.A., Day, A.H., Sharma, R.N. and Flay, R.G.J., 2016. The characterisation of the hydrodynamic loads on tidal turbines due to turbulence. *Renewable and Sustainable Energy Reviews*, *56*, pp.851-864 (doi.org/10.1016/j.rser.2015.11.095)

[5] Vinod, A. and Banerjee, A., 2019. Performance and near-wake characterization of a tidal current turbine in elevated levels of free stream turbulence. *Applied Energy*, 254, p.113639 (doi:10.1016/j.apenergy.2019.113639)

[6] Xie, T., Wang, T., He, Q., Diallo, D. and Claramunt, C., 2020. A review of current issues of marine current turbine blade fault detection. *Ocean Engineering*, *218*, p.108194 (doi.org/10.1016/j.oceaneng.2020.108194)

[7] Goss, Z.L., Coles, D.S., Kramer, S.C. and Piggott, M.D., 2021. Efficient economic optimisation of large-scale tidal stream arrays. *Applied Energy*, *295*, p.116975 (doi.org/10.1016/j.apenergy.2021.116975)

[8] Ouro, P. and Stoesser, T., 2019. Impact of environmental turbulence on the performance and loadings of a tidal stream turbine. *Flow, Turbulence and Combustion*, 102(3), pp.613-639 (doi:10.1007/s10494-018-9975-6)

[9] Mycek, P., Gaurier, B., Germain, G., Pinon, G. and Rivoalen, E., 2014. Experimental study of the turbulence intensity effects on marine current turbines

behaviour. Part I: One single turbine. *Renewable Energy*, *66*, pp.729-746 (doi.org/10.1016/j.renene.2013.12.036)

[10] Blackmore, T., Myers, L.E. and Bahaj, A.S., 2016. Effects of turbulence on tidal turbines: Implications to performance, blade loads, and condition monitoring. *International Journal of Marine Energy*, *14*, pp.1-26 (doi.org/10.1016/j.ijome.2016.04.017)

[11] Payne, G.S., Stallard, T., Martinez, R. and Bruce, T., 2018. Variation of loads on a three-bladed horizontal axis tidal turbine with frequency and blade position. *Journal of Fluids and Structures*, *83*, pp.156-170 (doi.org/10.1016/j.jfluidstructs.2018.08.010)

[12] Pacheco, A. and Ferreira, Ó., 2016. Hydrodynamic changes imposed by tidal energy converters on extracting energy on a real case scenario. Applied Energy, 180, pp.369-385 (doi:10.1016/j.apenergy.2016.07.132)

[13] MacEnri, J., Reed, M. and Thiringer, T., 2013. Influence of tidal parameters on SeaGen flicker performance. *Philosophical Transactions of the Royal Society A: Mathematical, Physical and Engineering Sciences*, *371*(1985), p.20120247 (doi.org/10.1098/rsta.2012.0247)

[14] Li, Y., Yi, J.H., Song, H., Wang, Q., Yang, Z., Kelley, N.D. and Lee, K.S., 2014. On the natural frequency of tidal current power systems—A discussion of sea testing. Applied Physics Letters, 105(2), p.023902 (doi:10.1063/1.4886797)

[15] Sentchev, A., Thiébaut, M. and Schmitt, F.G., 2020. Impact of turbulence on power production by a free-stream tidal turbine in real sea conditions. Renewable Energy, 147, pp.1932-1940 (doi:10.1016/j.renene.2019.09.136)

[16] Thiébaut, M. and Sentchev, A., 2015. Estimation of tidal stream potential in the Iroise Sea from velocity observations by high frequency radars. Energy Procedia, 76, pp.17-26 (doi:10.1016/j.egypro.2015.07.835)

[17] Guillou, N., Charpentier, J.F. and Benbouzid, M., 2020. The Tidal Stream Energy Resource of the Fromveur Strait—A Review. *Journal of Marine Science and Engineering*, *8*(12), p.1037 (doi.org/10.3390/jmse8121037)

[18] Bian, C., Liu, Z., Huang, Y., Zhao, L. and Jiang, W., 2018. On estimating turbulent Reynolds stress in wavy aquatic environment. Journal of Geophysical Research: Oceans, 123(4), pp.3060-3071 (doi:10.1002/2017JC013230)

[19] Perez, L., Cossu, R., Couzi, C. and Penesis, I., 2020. Wave-Turbulence Decomposition Methods Applied to Tidal Energy Site Assessment. Energies, 13(5), p.1245 (doi:10.3390/en13051245)

[20] Lu, Y. and Lueck, R.G., 1999. Using a broadband ADCP in a tidal channel. Part II: Turbulence. *Journal of Atmospheric and Oceanic Technology*, *16*(11), pp.1568-1579 (doi.org/10.1175/1520-0426(1999)016<1568:UABAIA>2.0.CO;2)

[21] Stacey, M.T., Monismith, S.G. and Burau, J.R., 1999. Measurements of Reynolds stress profiles in unstratified tidal flow. *Journal of Geophysical Research: Oceans*, *104*(C5), pp.10933-10949 (doi.org/10.1029/1998JC900095)

[22] Rippeth, T.P., Simpson, J.H., Williams, E. and Inall, M.E., 2003. Measurement of the rates of production and dissipation of turbulent kinetic energy in an energetic tidal flow: Red Wharf Bay revisited. *Journal of Physical Oceanography*, *33*(9), pp.1889-1901 (doi.org/10.1175/1520-0485(2003)033<1889:MOTROP>2.0.CO;2)

[23] Guerra, M. and Thomson, J., 2017. Turbulence measurements from five-beam acoustic Doppler current profilers. *Journal of Atmospheric and Oceanic Technology*, *34*(6), pp.1267-1284 (doi.org/10.1175/JTECH-D-16-0148.1)

[24] Pu, J.H., Tait, S., Guo, Y., Huang, Y. and Hanmaiahgari, P.R., 2018. Dominant features in three-dimensional turbulence structure: comparison of non-uniform accelerating and decelerating flows. *Environmental Fluid Mechanics*, *18*(2), pp.395-416 (doi.org/10.1007/s10652-017-9557-5)

[25] Thomson, J., Polagye, B., Durgesh, V. and Richmond, M.C., 2012. Measurements of turbulence at two tidal energy sites in Puget Sound, WA. IEEE Journal of Oceanic Engineering, 37(3), pp.363-374 (doi:10.1109/JOE.2012.2191656)

[26] Greenwood, C., Vogler, A. and Venugopal, V., 2019. On the variation of turbulence in a high-velocity tidal channel. *Energies*, *12*(4), p.672 (doi.org/10.3390/en12040672)

[27] Song, T. and Chiew, Y.M., 2001. Turbulence measurement in nonuniform open-channel flow using acoustic Doppler velocimeter (ADV). Journal of Engineering Mechanics, 127(3), pp.219-232 (doi:10.1061/(ASCE)0733-9399(2001)127:3(219)

[28] Williams, P., Roussinova, V. and Balachandar, R., 2018. Turbulence structure of non-uniform rough open channel flow. In E3S Web of Conferences (Vol. 40, p. 05039). EDP Sciences (doi:10.1051/e3sconf/20184005039)

[29] McCann, G., 2007, September. Tidal current turbine fatigue loading sensitivity to waves and turbulence–a parametric study. In Proceedings from 7th European wave and tidal energy conference.

[30] Maganga, F., Germain, G., King, J., Pinon, G. and Rivoalen, E., 2010. Experimental characterisation of flow effects on marine current turbine behaviour and on its wake properties. *IET Renewable Power Generation*, 4(6), pp.498-509 (doi:10.1049/iet-rpg.2009.0205)